Supplementary Information

Generation of active $Mn(III)_{(aq)}$ by a novel heterogeneous Electro-permanganate (E-PM) process with manganese(II) as promoter and stabilizer

Yunhua Zhu [a, b], Xuxu Wang [a, b], Jing Zhang [b], Lei Ding [d], Junfeng Li [c], Huaili Zheng [a, b], Chun Zhao [a, b, c*]

[a]State Key Laboratory of Coal Mine Disaster Dynamics and Control, Chongqing University, Chongqing 400044, PR China

[b]Key Laboratory of the Three Gorges Reservoir Region's Eco-Environment, Ministry of Education, Chongqing University, Chongqing 400045, PR China

[c]College of Water & Architectural Engineering, Shihezi University, Shihezi 832000, PR China

[d]School of Civil Engineering and Architecture, Anhui University of Technology, 59 Hudong Road, Maanshan 243002, PR China

*Corresponding author

Email: pureson@163.com; pureson@cqu.edu.cn

Contents

Text S1 Reagents and chemicals

DCF ($C_{14}H_{10}Cl_2NNaO_2$, purity 99.0%) was purchased from the Chengdu Micxy Chemical Co., Ltd. (China). Sulfamethoxazole (SMX, $C_{10}H_{11}N_3O_3S$, 99.0%) and methyl blue (MB, $C_{37}H_{27}N_3Na_2O_9S_3$) were supplied by Aladdin Chemical Co., Ltd. (China). Carbamazepine (CBZ) and HA were purchased from Sigma-Aldrich Chemical Co., Ltd. (USA). Phenol (C_6H_6O, purity 99.5%), nitrobenzene (NB, $C_6H_5NO_2$), potassium permanganate ($KMnO_4$, purity 99.5%), manganese sulphate ($MnSO_4•H_2O$, purity 99.0%), tert-butanol (TBA, $C_4H_{10}O$, purity 99.0%), formic acid (HPLC grade), and acetic acid (HPLC grade), were obtained from Chengdu Kelong Chemical Co., Ltd. (China). Methanol (MA) and acetonitrile (HPLC grade) were supplied by Honeywell Burdick & Jackson Inc. (USA). Sulfuric acid (H_2SO_4, 98.0%), sodium hydroxide (NaOH, purity 98.0%), hydroxylammonium chloride ($NH_2OH•HCl$, purity 98.5%), and sodium pyrophosphate decahydrate ($Na_4P_2O_7•10H_2O$, purity 99%), were obtained from Chongqing Chuandong Chemical Co., Ltd. (China). All sample solutions and mobile phase were prepared with ultrapure water (resistivity of 18.2 MΩ cm) obtained from Millipore Super-Q plus water purification system.

Text S2 The analytical method of the intermediate products

Considering the high detection limit, the intermediates samples were concentrated by solid phase extraction (SPE) prior to UPLC-Vion IMS QTOF-MS analysis. 20 mL solution sample was introduced into Oasis HLB cartridge (Waters, America), and eluted by 2mL pure methanol. Then the chromatographic separation was carried out on a BEH C_{18} (100 mM × 2.1 mM × 1.7 μM) maintained at 45 °C. The mobile phase consisted of A (0.1% formic acid in ultrapure water) and B (0.1% formic acid in acetonitrile) at a flow rate of 0.4 mL min^{-1}. The gradient was 95% A and 5% B at initial, then increasing to 100% B for 8 min and 12.5 min, changed to 5% A and 95% B for 15 min and 20 min. The injection volume was set to 1 μL. The mass spectrometer (m/z 50-1000) was operated with negative electrospray ionization. The MS operation parameters were set as follows: acquisition mode MS^E; capillary voltage 2 KV; cone voltage 40V; desolvation temperature 450 °C; desolvation gas 900 L h^{-1}; cone gas 50 L h^{-1}; source temperature 115 °C; Scan rate 0.2 s; Collision energy 6 eV/20-45 eV.

Text S3 Effect of adding time of Mn^{2+} on the degradation of DCF by E-PM-Mn^{2+} process in the presence of PP

To explore whether PP affects the reaction involving Mn(II) in the E-PM-Mn^{2+} process, UV-vis spectra of Mn^{2+} solution with and without PP and the comparative experiments according to the different adding time of Mn^{2+} were carried out.

As illustrated in Figure S10, UV-vis spectra of Mn^{2+} solution with and without PP (PP 10mM) had no obvious absorption peaks, although the concentration of Mn^{2+} had increased to 10 to 100 folds. However, an obvious absorbance peak of Mn(III)-PP at 258 nm was observed in E-PM-Mn^{2+} process (Figure S7(c)). The phenomena indicated that the complex had little effect on the generation of Mn(III) and the UV-vis spectra of Mn(III)-PP, even if Mn^{2+} complexed with PP.

The comparative experiments according to the different adding time of Mn^{2+} in E-PM-Mn^{2+} process were explored. In the experiment A, the solution including PP, DCF and Na_2SO_4 (the supporting electrolyte) was adjusted using H_2SO_4 or NaOH to 5, and then as the DC power supply was turned on, PM and Mn^{2+} were immediately spiked into the solution simultaneously, which was the experiment order in the manuscript. In the experiment B, Mn^{2+} was first added into the solution containing PP, DCF, and Na_2SO_4, and initial pH of solution was adjusted using H_2SO_4 or NaOH to 5, and then as the DC power supply was turned on, PM was immediately spiked into the solution simultaneously. Mn^{2+} and PP were sufficiently in contact with each other.

The conditions of the two experiments were same, except for the adding time of Mn^{2+}. As shown in Figure S10, different adding time of Mn^{2+} had negligible effect on DCF

degradation by E-PM-Mn^{2+} process in the presence of PP. Therefore, these results indicated that the influence of PP on the degradation reaction involving Mn(II) in the E-PM-Mn^{2+} was negligible in this study.

Text S4 The calculation formula of synergetic effect

$$SE = \frac{k_1(E - PM - Mn^{2+})}{k_1(E - Mn^{2+}) + k_1(PM)} \quad (S1)$$

where SE is the synergetic index, k(E-PM-Mn^{2+}), k(E-Mn^{2+}), and k(PM) are the pseudo-first-order rate constants of E-PM-Mn^{2+}, E-Mn^{2+}, and PM processes, respectively (obtained in Figure 1(a) and the inset of Figure 4(d), s^{-1}).

Table S1. Water quality parameters of the electrolyte solution, tap water, and surface water.

Constituent	electrolyte solution	Tap water	Surface water
pH	7.00	7.78	7.44
DOC(mg/L)	0	1.08	10.5
$UV_{254}(cm^{-1})$	-	0.043	0.182
CO_3^{2-}(mg/L)	-	0.83	1.89
HCO_3^-(mg/L)	-	104	150
Cl^-(mg/L)	-	6.6	13.1
SO_4^{2-}(mg/L)	0	104.1	150.1
PO_4^{3-}(mg/L)	-	1.63	4.35
NO_3^-(mg/L)	-	2.03	1.54
Ammonia (mg-N/L)	-	-	1.84

141 Table S2. Details for contaminants analyses by HPLC-UV

Contaminants	Column temperature (°C)	Mobile phase (v)					UV wavelength (nm)
		water (%)	methanol (%)	acetonitrile (%)	0.1% formic acid	3% acetic acid	
Diclofenac (DCF)	30			80		20	276
Carbamazepine (CBZ)	35	40		60			286
Sulfamethoxazole (SMX)	35			38	62		265
Nitrobenzene (NB)	35	35	50	15			262
phenol	30	20	80				270

143 Table S3. The comparison of the E-PM-Mn^{2+} process with the other methods for the

144 degradation of DCF

System	DCF concentration	solution pH	Degradation rate	Kinetic constant	Reference
$CoFe_2O_4$/oxone system	10 mg L^{-1}	5.0	99 % in 30 min	13.8 s^{-1}	1
Photoelectrocatalytic system	5 mg L^{-1}	6.23	71.9% in 6 h	0.0036 s^{-1}	2
Pyrite nanoparticles	25 mg L^{-1}	3.0	100% in 3 min	0.461 s^{-1}	3
hydrodynamic cavitation in conjunction with UV/TiO_2/H_2O_2	20 mg L^{-1}	4.0	94.78% in 120 min	1.56 s^{-1}	4
UV-activated persulfate process	8.88 mg L^{-1}	6.0	83% in 60 min	5.0×10^{-4} s^{-1}	5
pulsed corona discharge system	5 mg L^{-1}	6.0	100% in 10 min	-	6
Fenton reaction system	5 mg L^{-1}	4.0	95% in 180 s	0.164 s^{-1}	7
ultrasonic irradiation	14.81 mg L^{-1}	7.0	67% in 80 min	1.79 s^{-1}	8
Ozone and photolytic TiO_2 catalysed processes	29.62 mg L^{-1}	5.0	90% in 10 min	-	9
Activated carbon-free ozonation	30 mg L^{-1}	7.0	100% in 15 min	-	10
US/ZnO	10 mg L^{-1}	2.0	85% in 15 min	-	11
Photoelectro-oxidation	10 mg L^{-1}	5.6	85% in 2h	0.0191 s^{-1}	12
E-PM-Mn^{2+}	6 mg L^{-1}	5.0	99.3% in 30 min	9.7314 s^{-1}	This work

145

Table S4. Kinetic parameters (k_1) and the correlation coefficients (R^2) of pseudo-first-order kinetics for DCF degradation in MnO_2, MnO_2-Mn^{2+}, E-MnO_2, and E-MnO_2-Mn^{2+} processes

constant	MnO_2	MnO_2-Mn^{2+}	E-MnO_2	E-MnO_2-Mn^{2+}
k_1 (s^{-1})	0.1032	0.1098	0.3342	0.6594
R^2	0.8579	0.8272	0.8610	0.9352

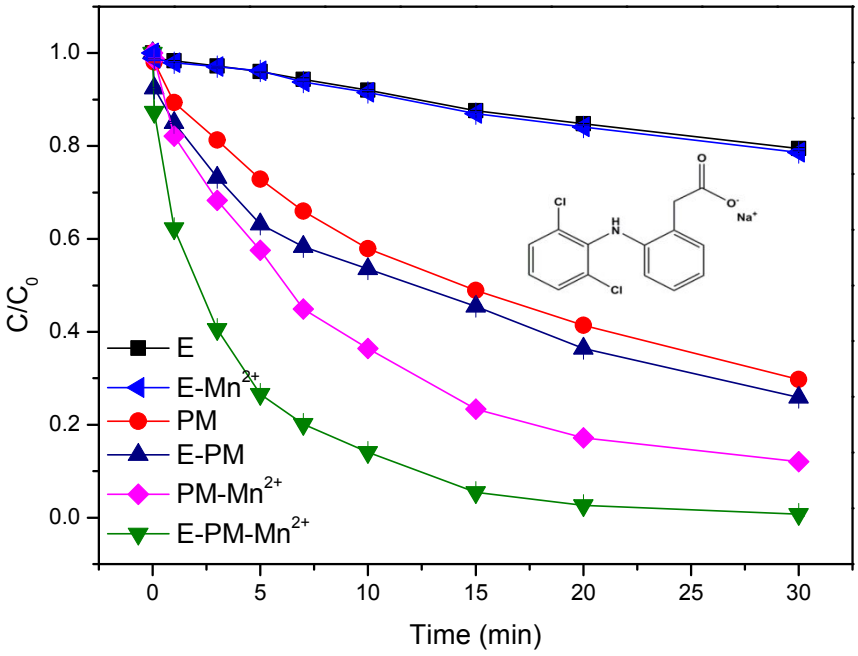

Figure S1. The degradation of DCF by electrolysis, PM oxidation, E-PM, E-Mn^{2+}, PM-Mn^{2+}, and E-PM-Mn^{2+} processes (Reaction conditions: initial DCF concentration=20 μM; initial pH=5; T=298±1 K; current=57 A m^{-2}; stirring speed=800 rpm; Mn^{2+} dosage=10 μM; PM dosage=100 μM).

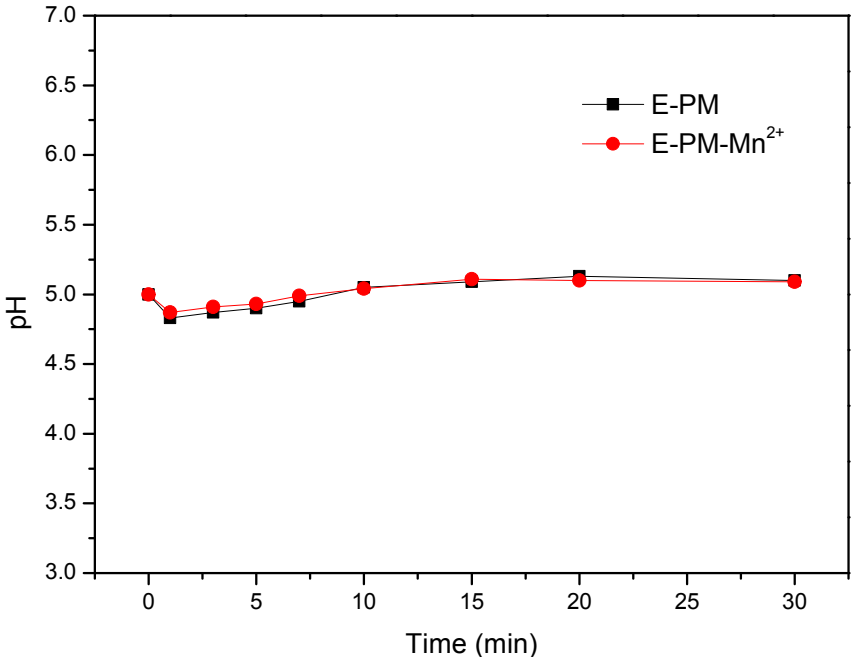

Figure S2. pH variations of solution on the removal of DCF by E-PM and E-PM-Mn^{2+} processes (Reaction conditions: initial DCF concentration=20 μM; T=298±1 K; stirring speed=800 rpm; PM dosage=100 μM; initial pH=5; Mn^{2+} dosage=10 μM)

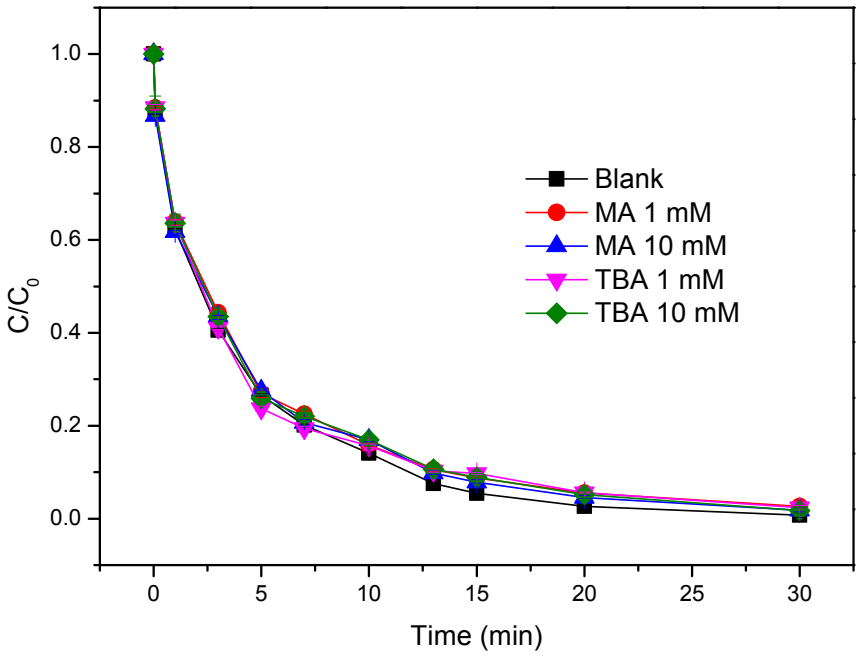

159

160 Figure S3. Effect of Methanol and TBA on DCF degradation by E-PM-Mn^{2+} process

161 (Reaction conditions: initial DCF concentration=20 μM; initial pH=5; T=298±1 K;

162 stirring speed=800 rpm; current=57 A m^{-2}; Mn^{2+} dosage=10 μM; PM dosage=100 μM).

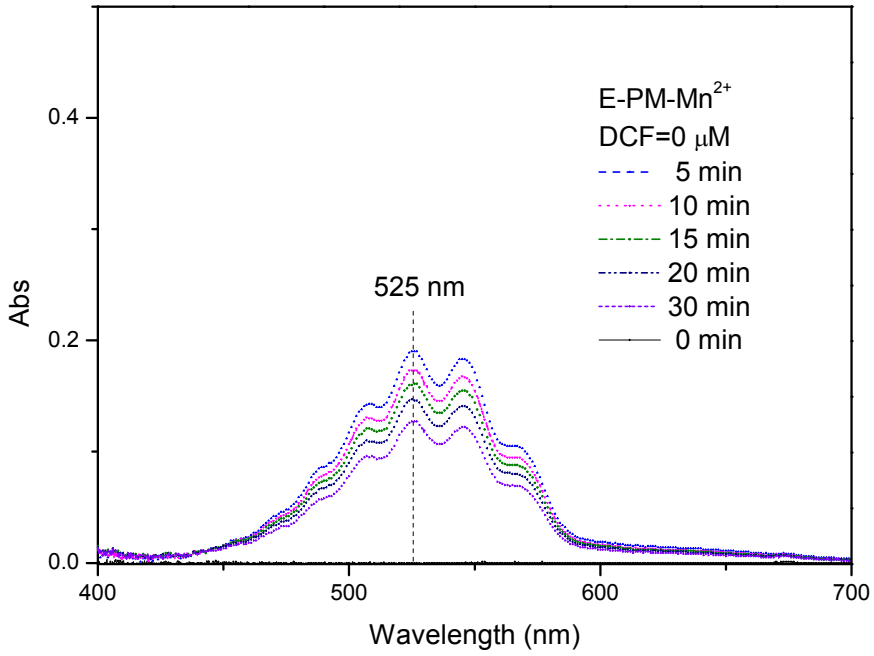

163

164 Figure S4. UV-vis spectra of E-PM-Mn^{2+} process without contaminants (Reaction

165 conditions: initial pH=5; T=298±1 K; current=57 A m^{-2}; stirring speed=800 rpm; PM

166 dosage=100 μM; Mn^{2+} dosage=10 μM).

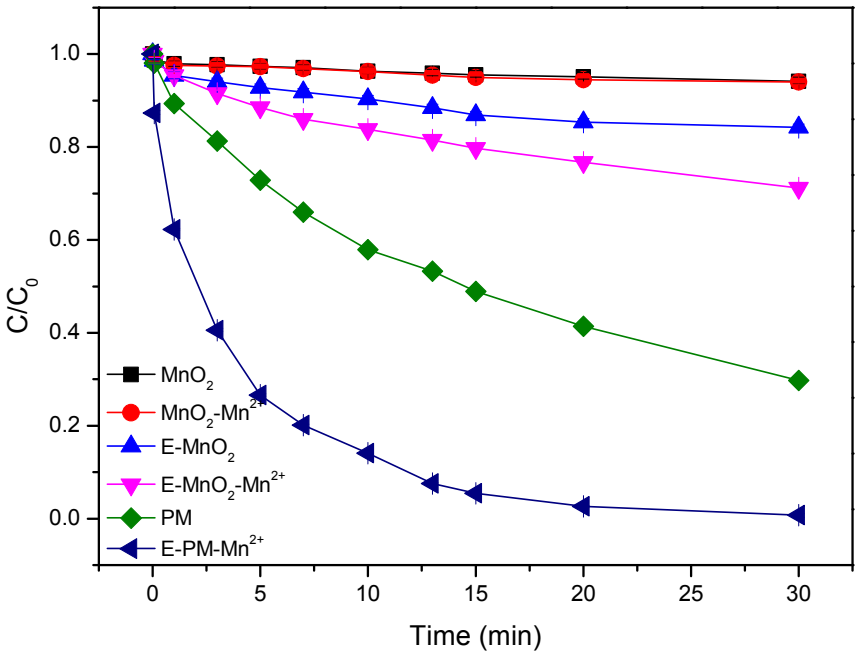

Figure S5. Comparative removal of DCF by MnO_2, MnO_2-Mn^{2+}, E-MnO_2, E-MnO_2-Mn^{2+}, PM, and E-PM-Mn^{2+} processes (Reaction conditions: initial DCF concentration=20 μM; initial pH=5; T=298±1 K; current=57 A m^{-2}; stirring speed=800 rpm; PM dosage=100 μM; MnO_2 dosage=100 μM, Mn^{2+} dosage=10 μM).

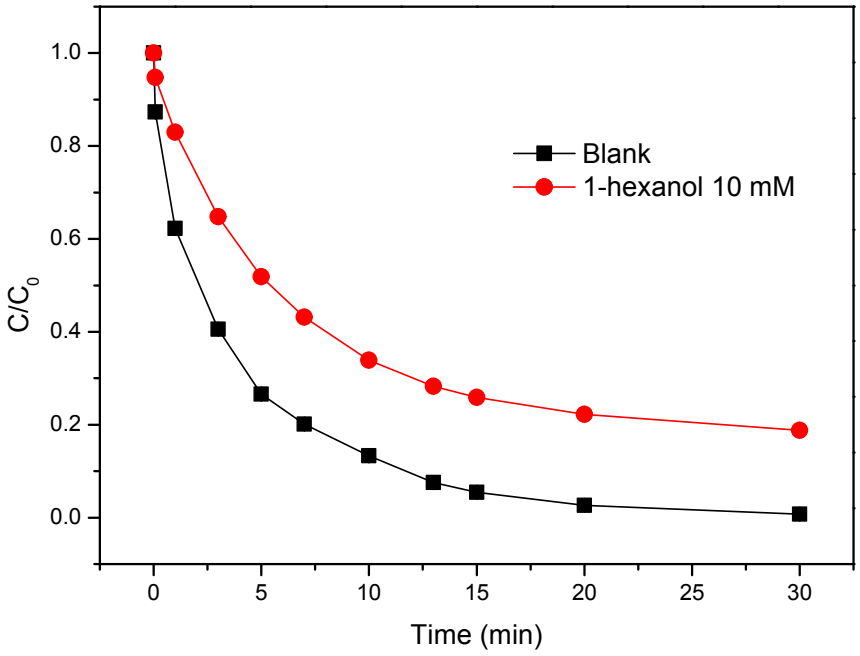

Figure S6. Effect of 1-hexanol on DCF degradation by E-PM-Mn^{2+} process (Reaction conditions: initial DCF concentration=20 μM; initial pH=5; T=298±1 K; stirring speed=800 rpm; current=57 A m^{-2}; Mn^{2+} dosage=10 μM; PM dosage=100 μM).

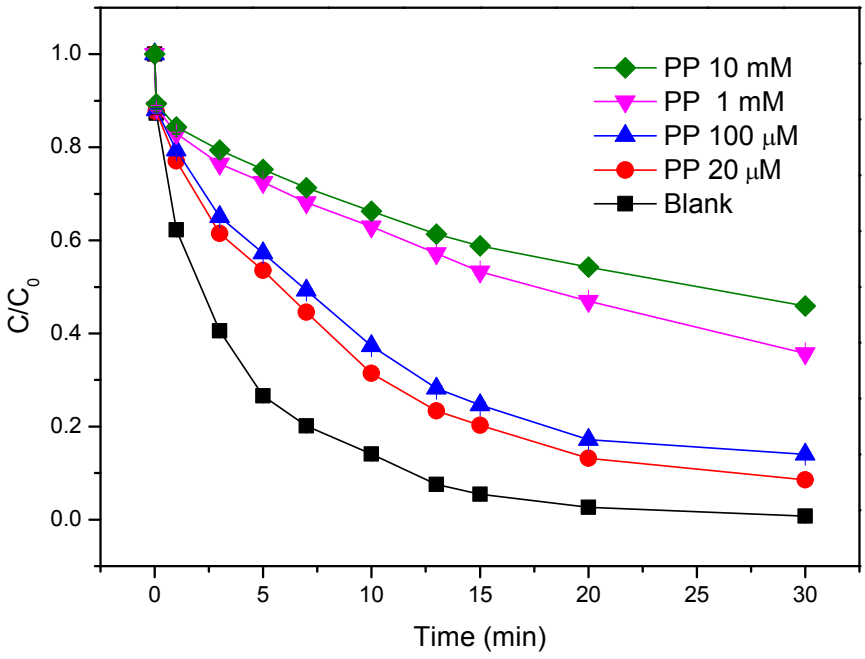

176

177 Figure S7. Effect of pyrophosphate (PP) on DCF degradation in E-PM-Mn^{2+} process

178 (Reaction conditions: initial DCF concentration=20 μM; initial pH=5; T=298±1 K;

179 stirring speed=800 rpm; current=57 A m^{-2}; Mn^{2+} dosage=10 μM; PM dosage=100 μM).

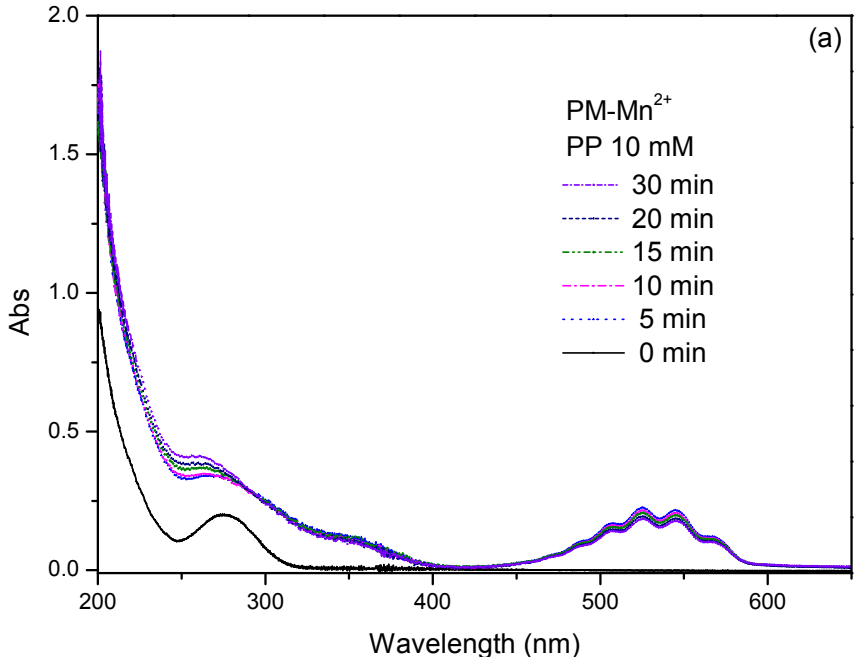
(a)
PM-Mn2+
PP 10 mM
30 min
20 min
15 min
10 min
5 min
0 min
Abs
Wavelength (nm)
2.0
1.5
1.0
0.5
0.0
200
300
400
500
600

180

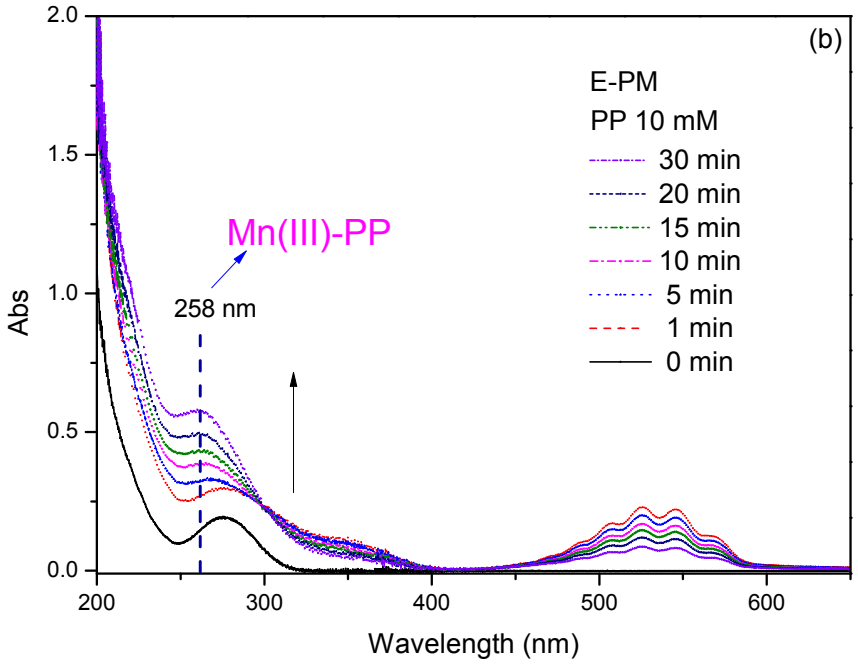
(b)
E-PM
PP 10 mM
30 min
20 min
15 min
10 min
5 min
1 min
0 min
Mn(III)-PP
258 nm
Abs
Wavelength (nm)
2.0
1.5
1.0
0.5
0.0
200
300
400
500
600

181

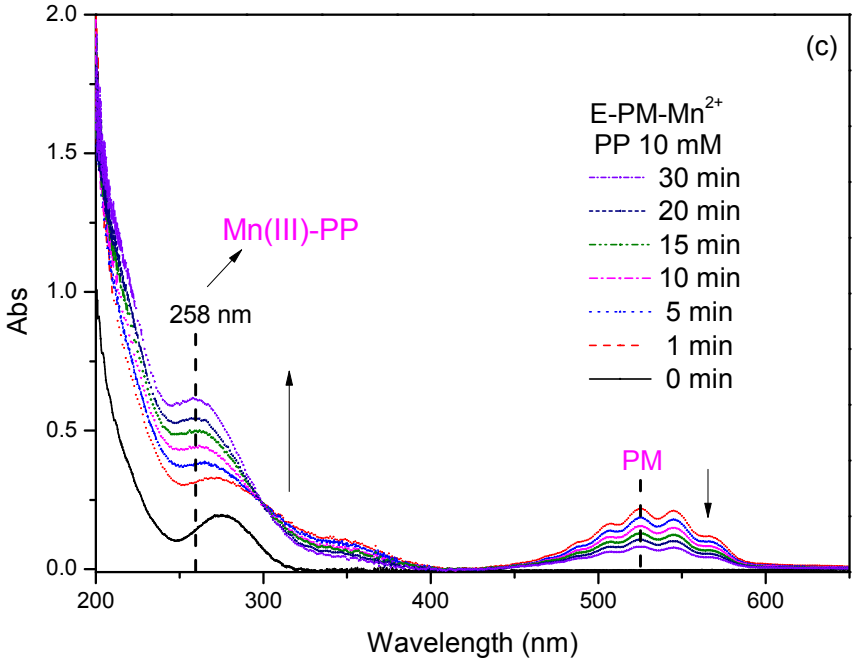

182

183 Figure S8. UV-vis spectra of Mn(III)-PP in PM-Mn^{2+} (a), E-PM (b) and E-PM-Mn^{2+} (c)

184 processes for DCF removal (Reaction conditions: initial DCF concentration=20 μM;

185 initial pH=5; T=298±1 K; current=57 A m^{-2}; stirring speed=800 rpm; PM dosage=100

186 μM; Mn^{2+} dosage=10 μM; PP dosage=10 mM).

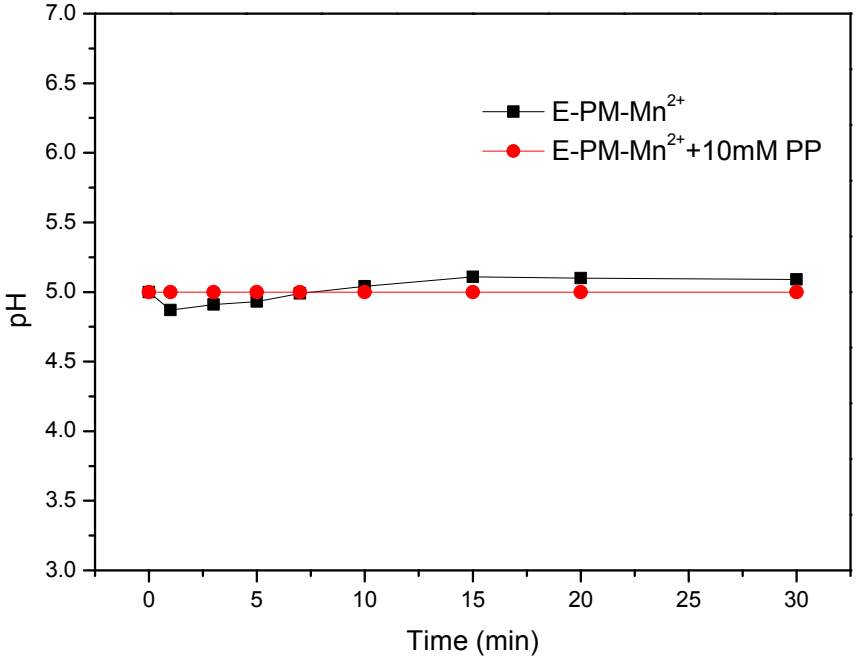

187

188 Figure S9. pH variations of solution on the removal of DCF by E-PM-Mn^{2+} process

189 with and without PP (Reaction conditions: initial DCF concentration=20 μM; T=298±1

190 K; stirring speed=800 rpm; PM dosage=100 μM; Mn^{2+} dosage=10 μM; initial pH=5;

191 PP dosage=10 mM)

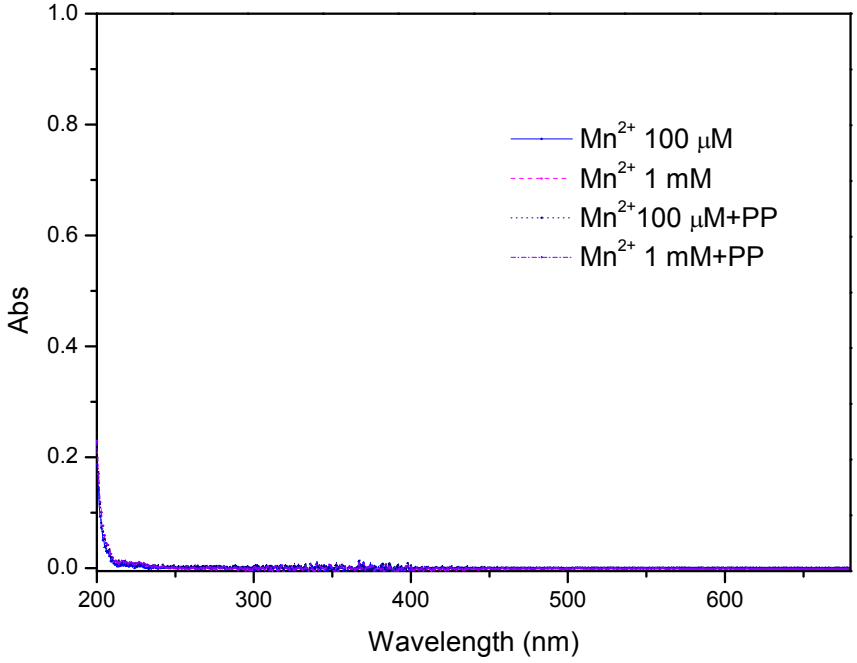

Figure S10. UV-vis spectra in Mn^{2+} solution with and without PP (Reaction conditions: initial pH=5; T=298±1 K; PP dosage=10 mM).

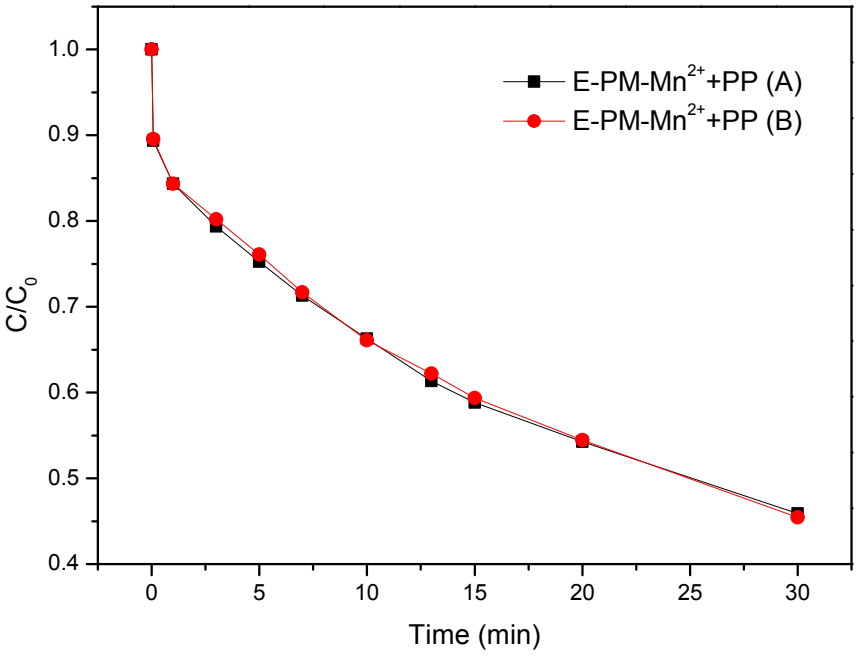

196

197 Figure S11. Effect of adding time of Mn^{2+} on the degradation of DCF by E-PM-Mn^{2+}

198 process in the presence of PP (Reaction conditions: initial DCF concentration=20 μM;

199 initial pH=5; T=298±1 K; current=57 A m^{-2}; stirring speed=800 rpm; PM dosage=100

200 μM; Mn^{2+} dosage=10 μM; PP dosage=10 mM).

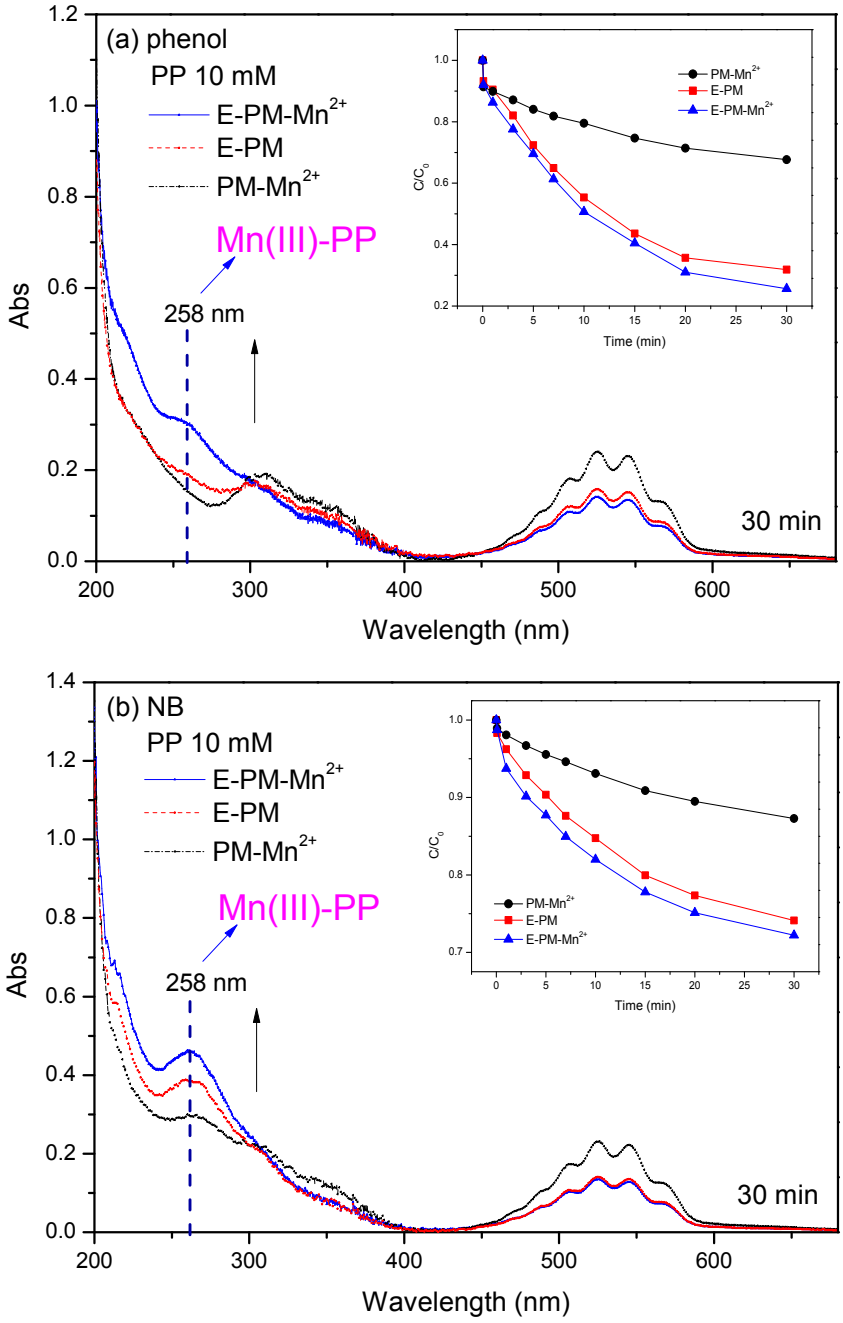

Figure S12. UV-vis spectra of Mn(III)-PP at 30 min in PM-Mn^{2+}, E-PM, and E-PM-Mn^{2+} processes for the degradation of phenol (a) and NB (b) (the insets showed the degradation of phenol and NB in PM-Mn^{2+}, E-PM, and E-PM-Mn^{2+} processes) (Reaction conditions: initial contaminant concentration=20 μM; initial pH=5; T=298±1 K; current=57 A m^{-2}; stirring speed=800 rpm; PM dosage=100 μM; Mn^{2+} dosage=10 μM; PP dosage=10 mM).

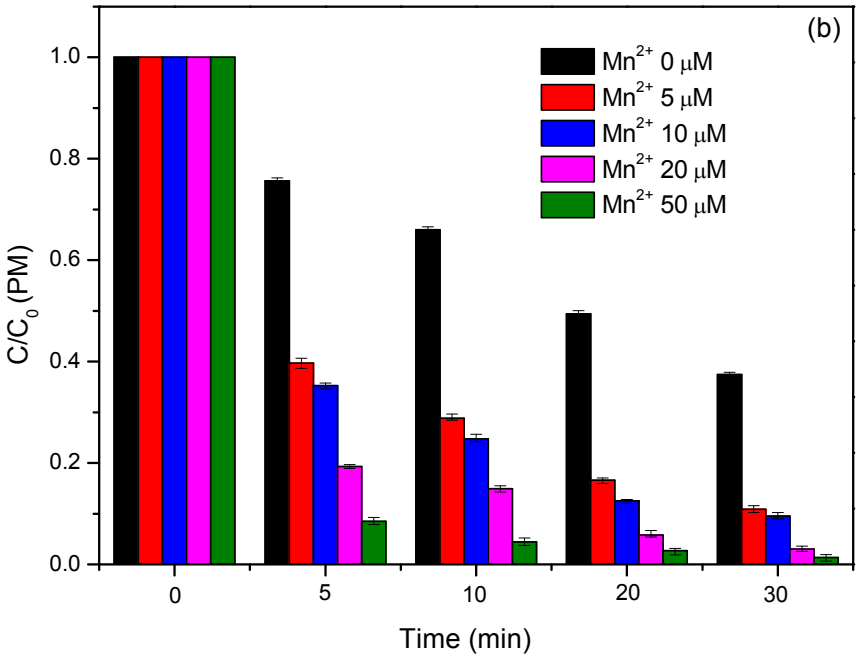

209

210 Figure S13. Effect of Mn^{2+} dosage on the PM decomposition by E-PM-Mn^{2+} process

211 (Reaction conditions: initial DCF concentration=20 μM; initial pH=5; T=298±1 K;

212 current=57 A m^{-2}; stirring speed=800 rpm; PM dosage=100 μM)

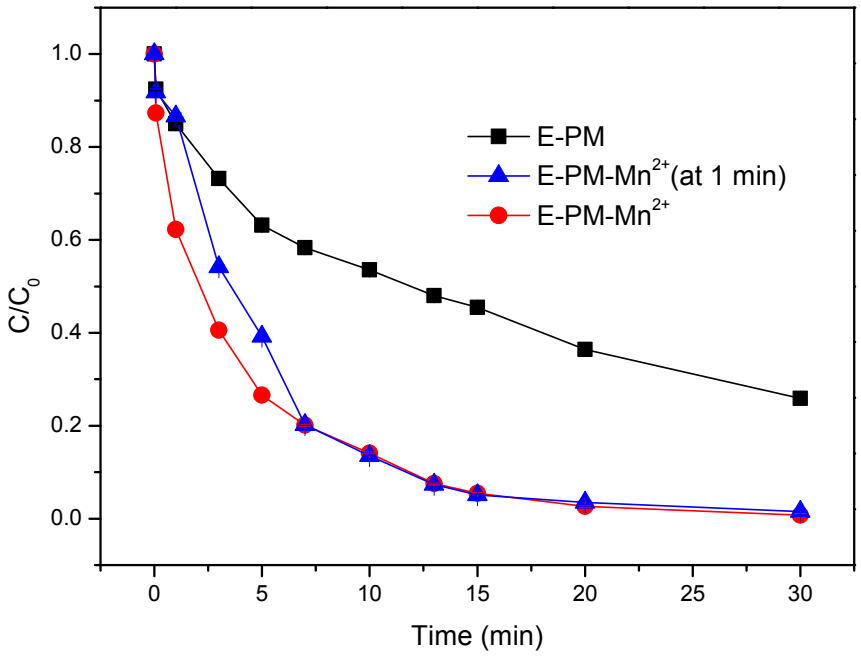

213

214 Figure S14. Influence of Mn^{2+} and the addition time on the removal of DCF by E-PM

215 and E-PM-Mn^{2+} processes (adding $MnSO_4$ at the beginning and at 1 min, respectively)

216 (Reaction conditions: initial DCF concentration=20 μM; initial pH=5; T=298±1 K;

217 stirring speed=800 rpm; current=57 A m^{-2}; PM dosage=100 μM; Mn^{2+} dosage=10 μM).

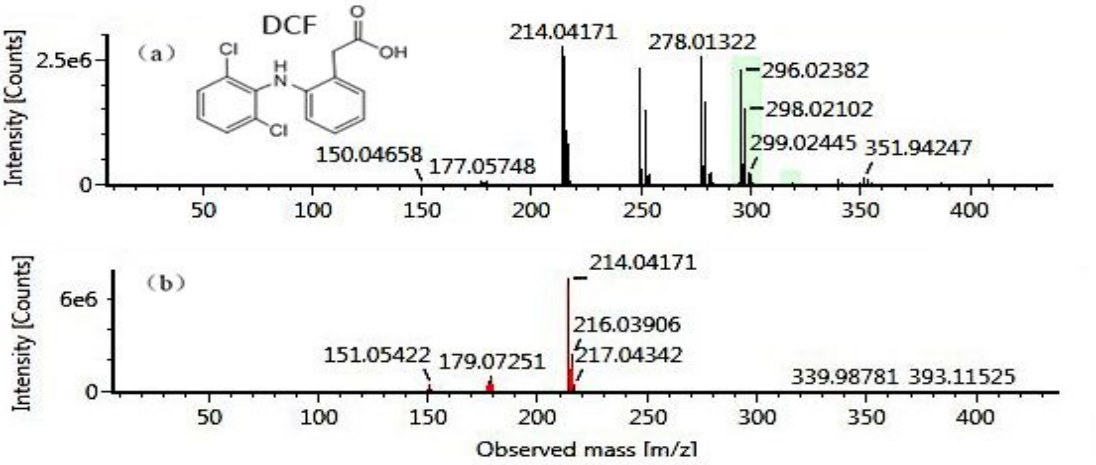
DCF
(a)
Cl
H
N
Cl
O
OH
214.04171
278.01322
296.02382
298.02102
299.02445
351.94247
150.04658
177.05748
Intensity [Counts]
2.5e6
0
50
100
150
200
250
300
350
400
(b)
214.04171
216.03906
217.04342
151.05422
179.07251
339.98781
393.11525
6e6
Observed mass [m/z]

218

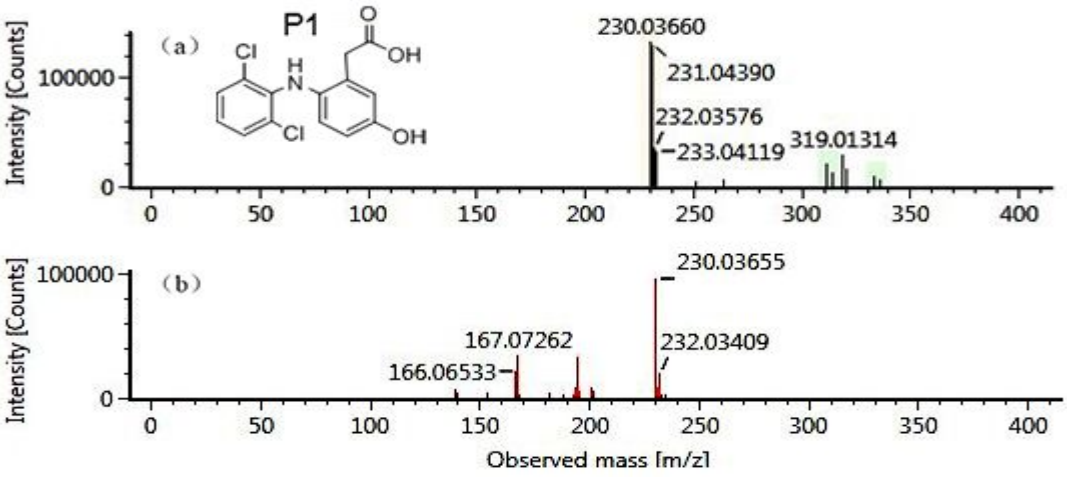
P1
(a)
Cl
H
N
Cl
O
OH
OH
230.03660
231.04390
232.03576
233.04119
319.01314
Intensity [Counts]
100000
0
50
100
150
200
250
300
350
400
(b)
230.03655
167.07262
232.03409
166.06533
Observed mass [m/z]

219

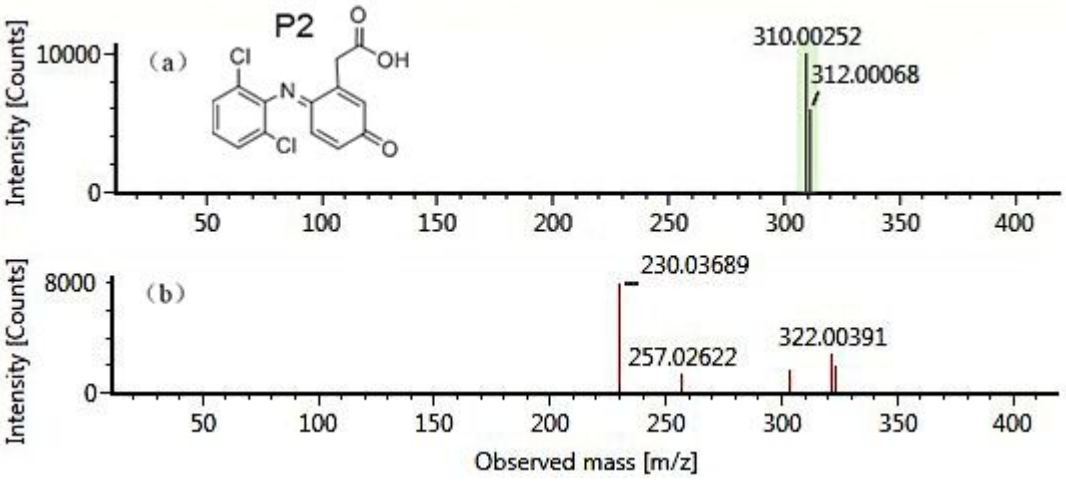
P2
(a)
Cl
N
Cl
O
OH
O
310.00252
312.00068
Intensity [Counts]
10000
0
50
100
150
200
250
300
350
400
(b)
230.03689
257.02622
322.00391
8000
Observed mass [m/z]

220

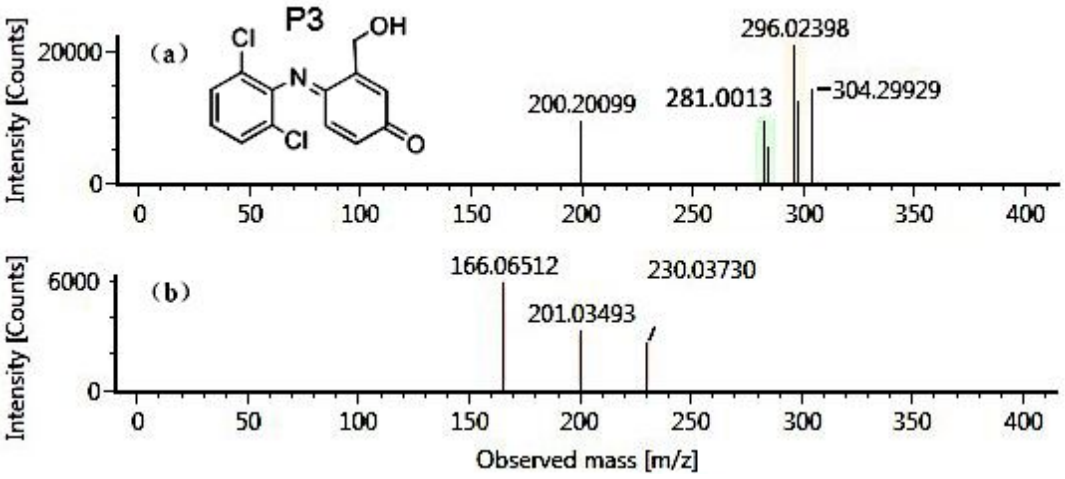
P3
(a)
Cl
N
Cl
OH
O
296.02398
200.20099
281.0013
304.29929
Intensity [Counts]
20000
0
0
50
100
150
200
250
300
350
400
(b)
166.06512
230.03730
201.03493
6000
Observed mass [m/z]

221

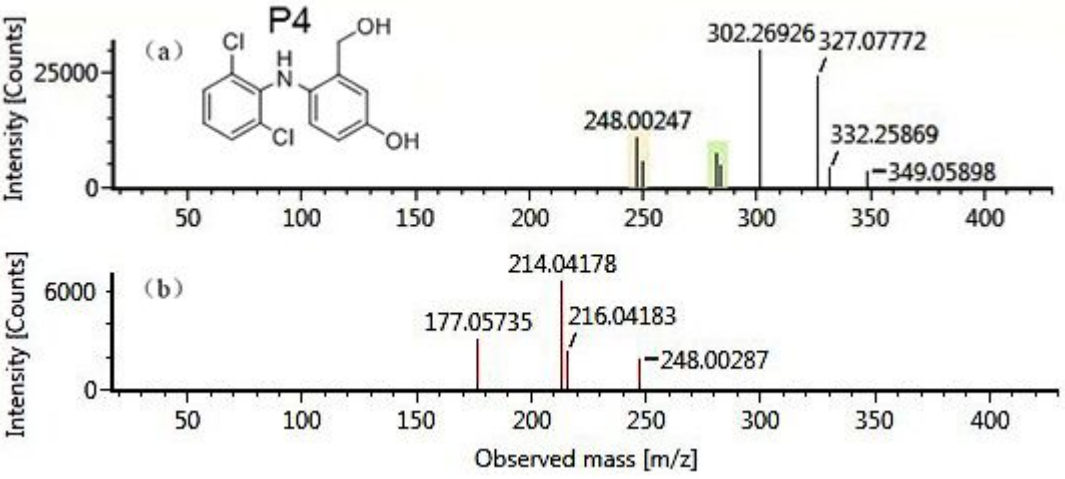
P4
(a)
Cl
H
N
Cl
OH
OH
302.26926
327.07772
248.00247
332.25869
349.05898
Intensity [Counts]
25000
0
50
100
150
200
250
300
350
400
(b)
214.04178
177.05735
216.04183
248.00287
6000
Observed mass [m/z]

222

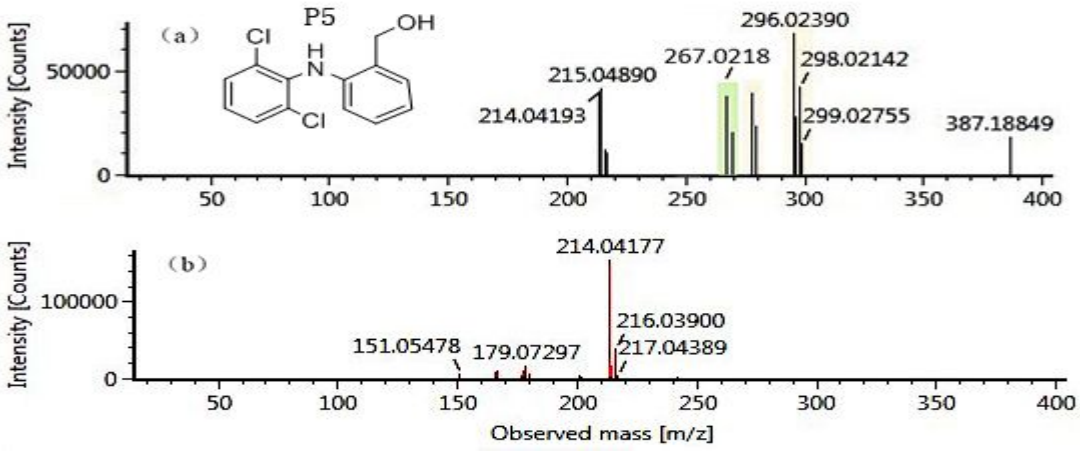
P5
(a)
Cl
H
N
Cl
OH
296.02390
267.0218
298.02142
215.04890
214.04193
299.02755
387.18849
Intensity [Counts]
50000
0
50
100
150
200
250
300
350
400
(b)
214.04177
216.03900
217.04389
151.05478
179.07297
100000
Observed mass [m/z]

223

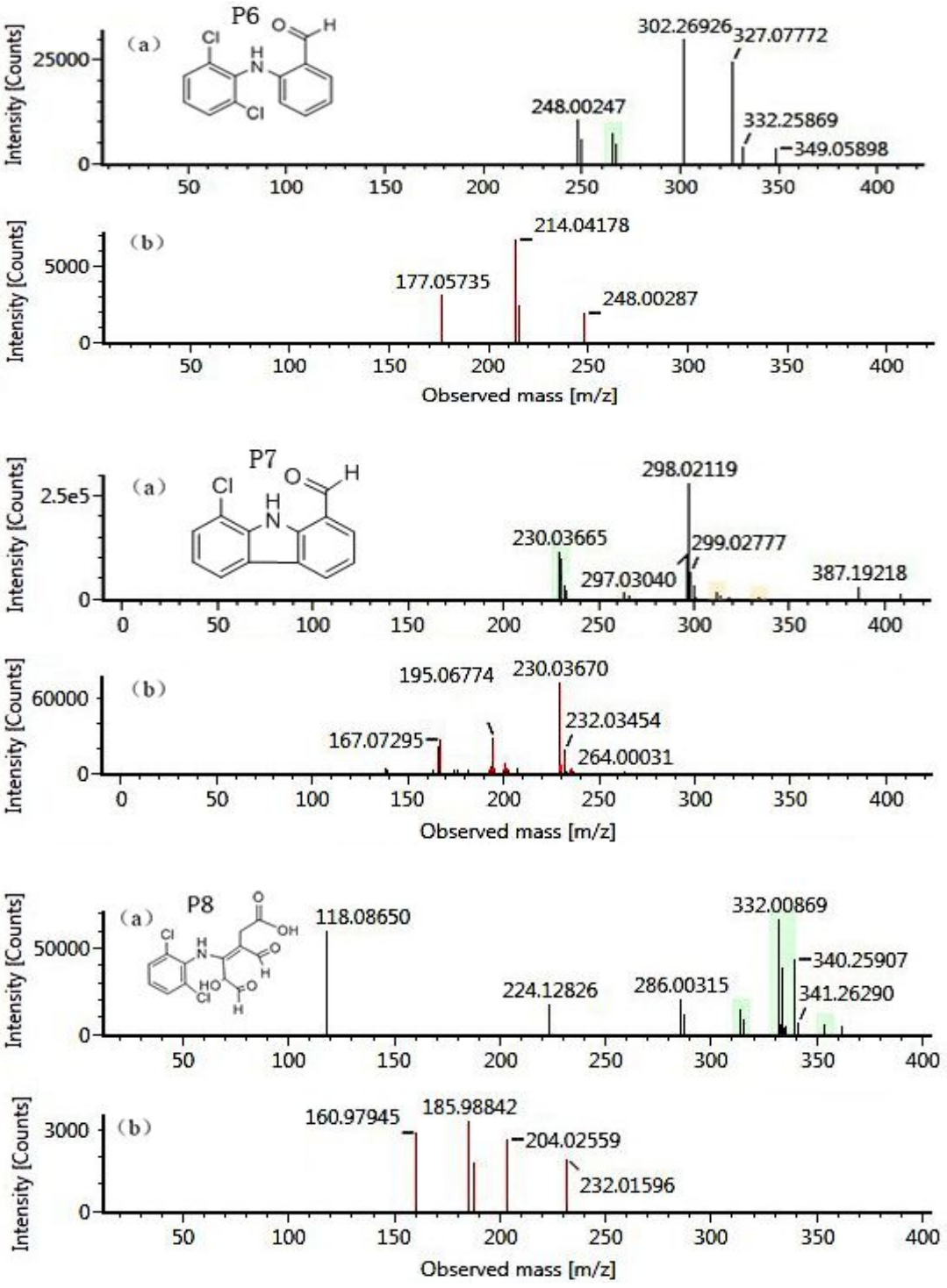

Figure S15. The product ion spectra (a) and the corresponding fragment ion spectra (b) for DCF and its degradation products (P1-P8) detected by UPLC-Vion IMS QTOF-MS (Reaction conditions: initial DCF concentration=20 μM; initial pH=5; T=298±1 K; current=57 A m^{-2}; stirring speed=800 rpm; PM dosage=100 μM; Mn^{2+} dosage=10 μM; reaction time=0-30 min).

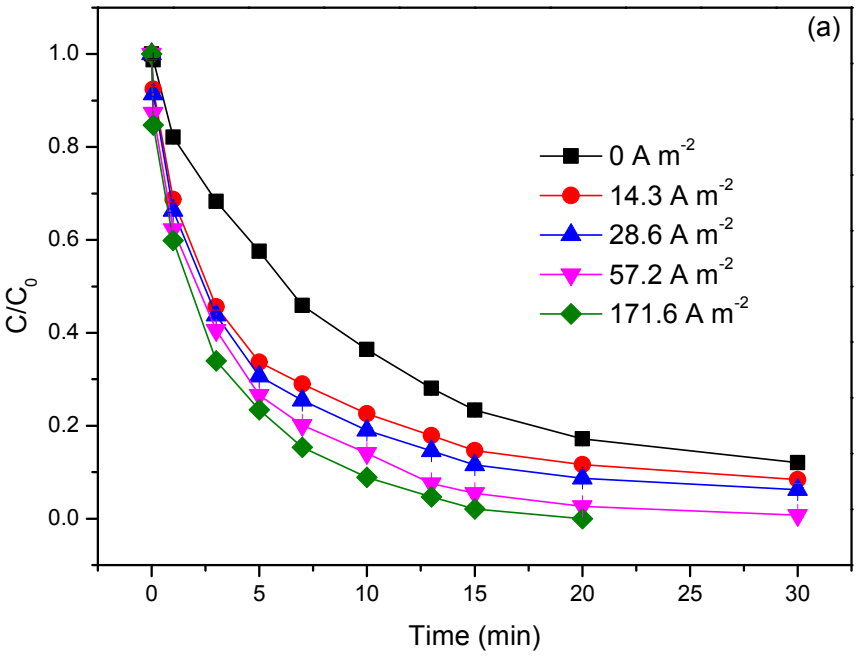
(a)
C/C0
Time (min)
0 A m-2
14.3 A m-2
28.6 A m-2
57.2 A m-2
171.6 A m-2

232

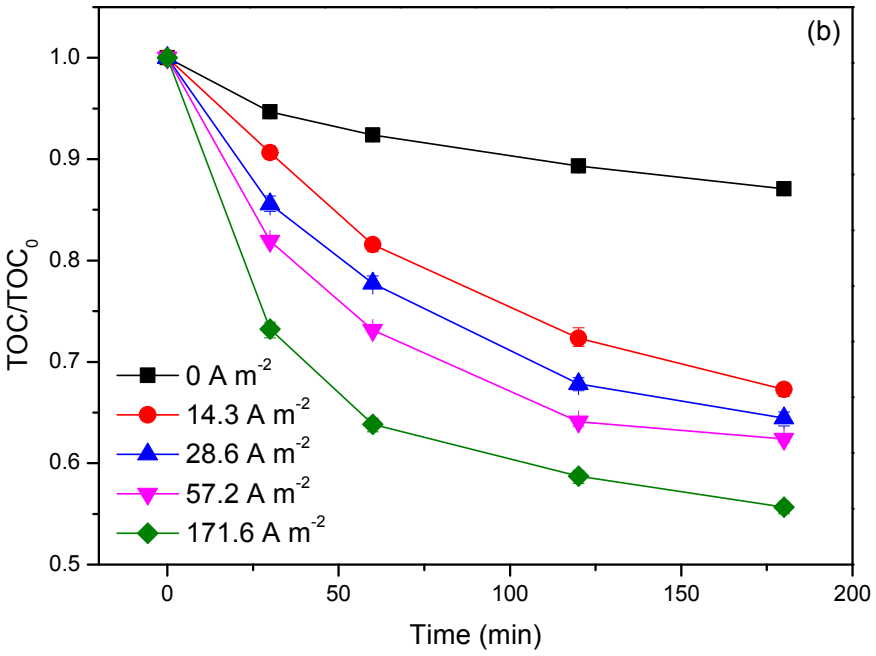
(b)
TOC/TOC0
Time (min)
0 A m-2
14.3 A m-2
28.6 A m-2
57.2 A m-2
171.6 A m-2

233

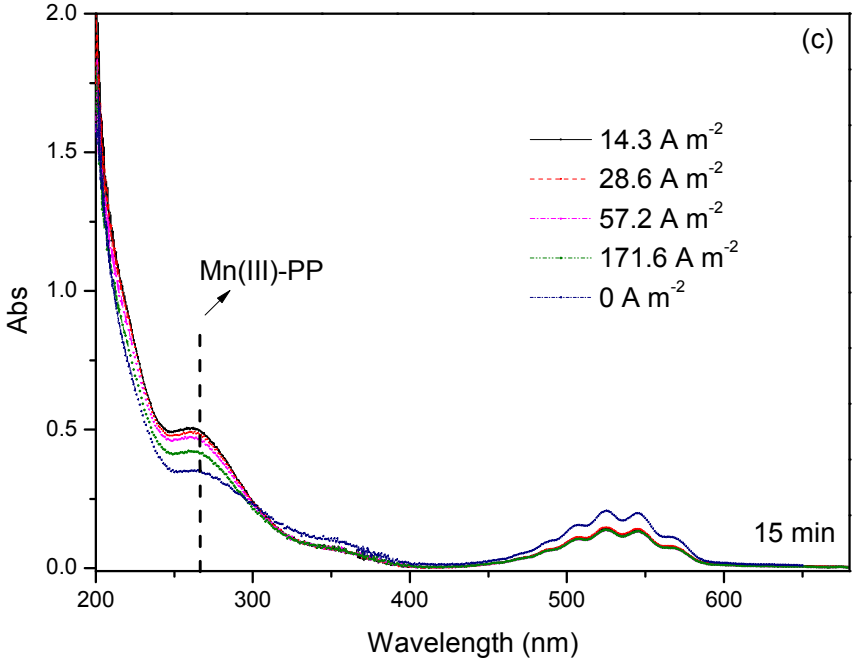

234

235 Figure S16. Effect of applied current on the DCF degradation (a), TOC removal (b) and

236 the Mn(III)-PP generation (c) in E-PM-Mn^{2+} process (Reaction conditions: initial DCF

237 concentration=20 μM; initial pH=5; T=298±1 K; stirring speed=800 rpm; PM

238 dosage=100 μM; Mn^{2+} dosage=10 μM; PP dosage=10 mM)

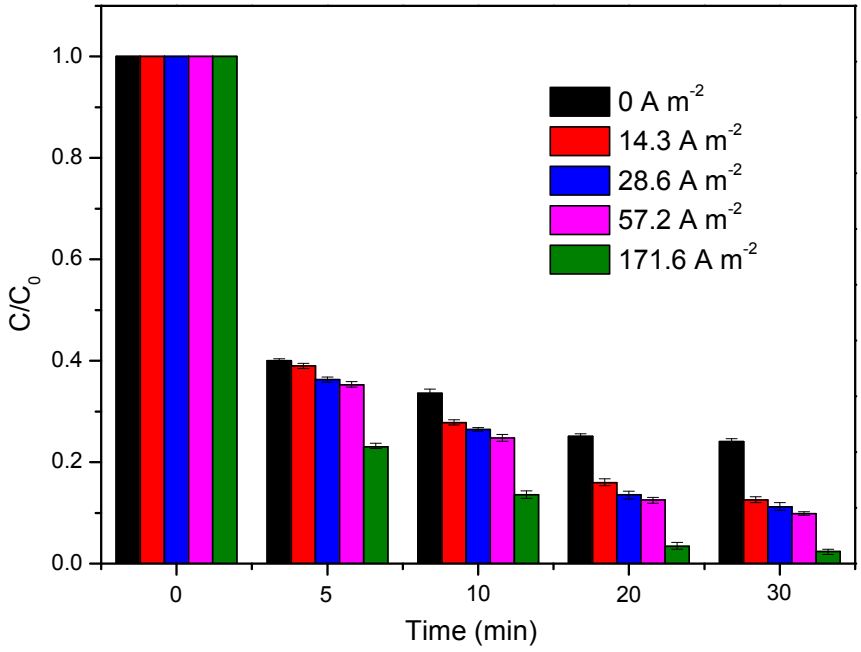

239

240 Figure S17. Effect of applied current on the decomposition of PM for DCF degradation

241 in E-PM-Mn^{2+} process (Reaction conditions: initial DCF concentration=20 μM; initial

242 pH=5; T=298±1 K; stirring speed=800 rpm; PM dosage=100 μM; Mn^{2+} dosage=10

243 μM)

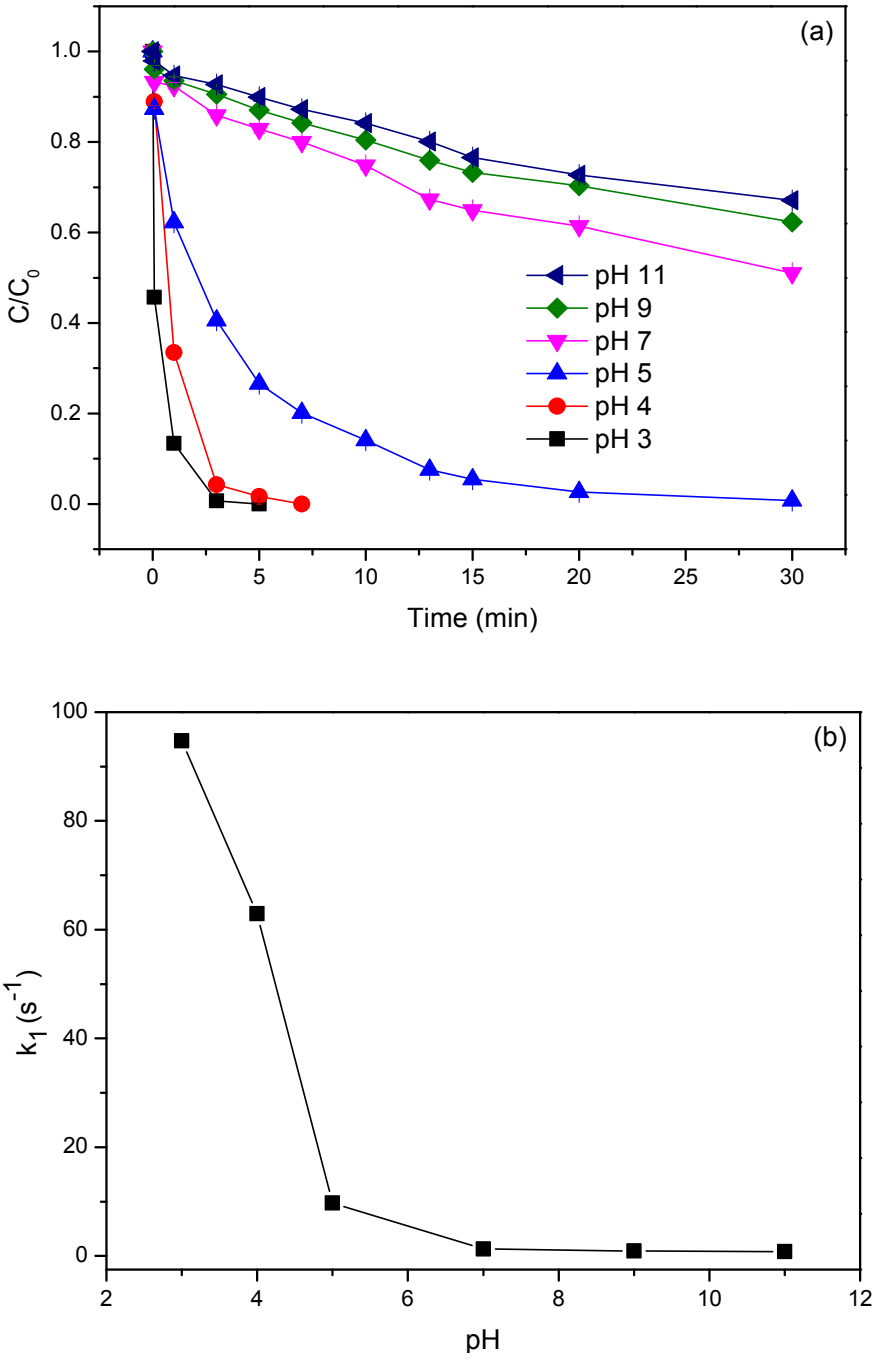

Figure S18. Effect of initial pH and the corresponding k_1 on the removal of DCF in E-PM-Mn^{2+} process (Reaction conditions: initial DCF concentration=20 μM; T=298±1 K; current=57 A m^{-2}; stirring speed=800 rpm; PM dosage=100 μM; Mn^{2+} dosage=10 μM)

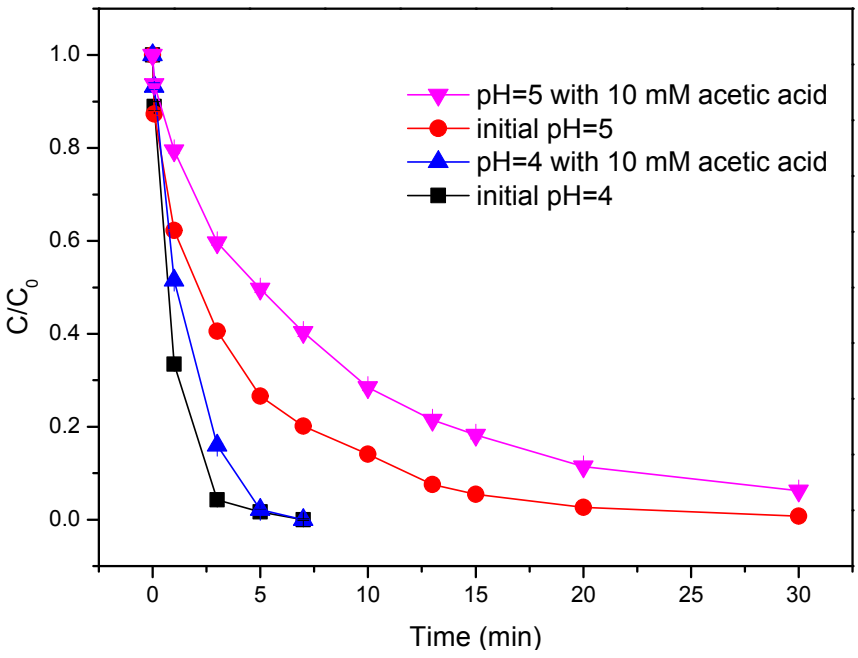

Figure S19. The effect of buffers on the removal of DCF in E-PM-Mn^{2+} process at pH 4 and 5 (Reaction conditions: initial DCF concentration=20 μM; T=298±1 K; stirring speed=800 rpm; PM dosage=100 μM; Mn^{2+} dosage=10 μM; constant pH 4 and 5 adjusted by 10 mM acetic acid dosage; initial pH adjusted using 0.1 M or 1 M H_2SO_4 and NaOH).

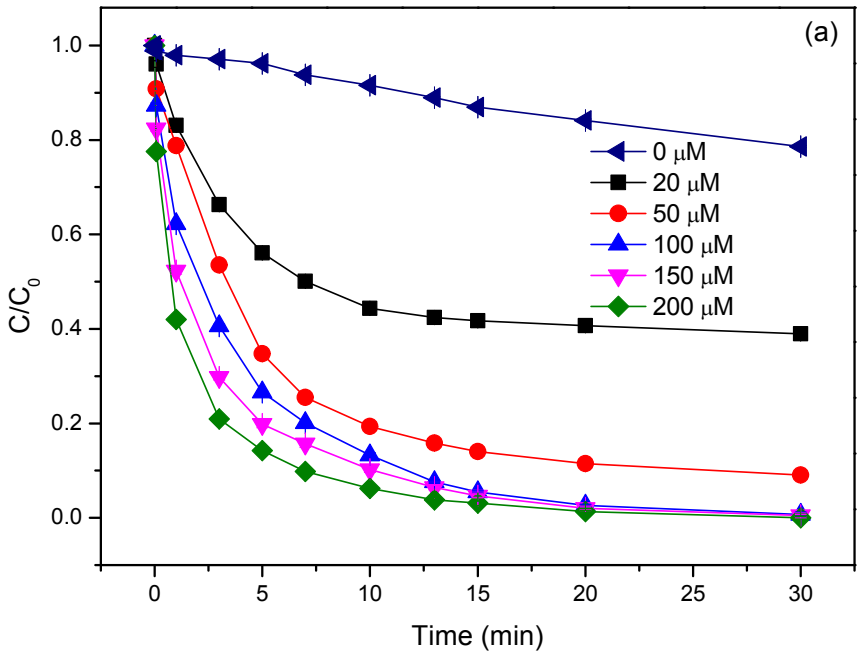

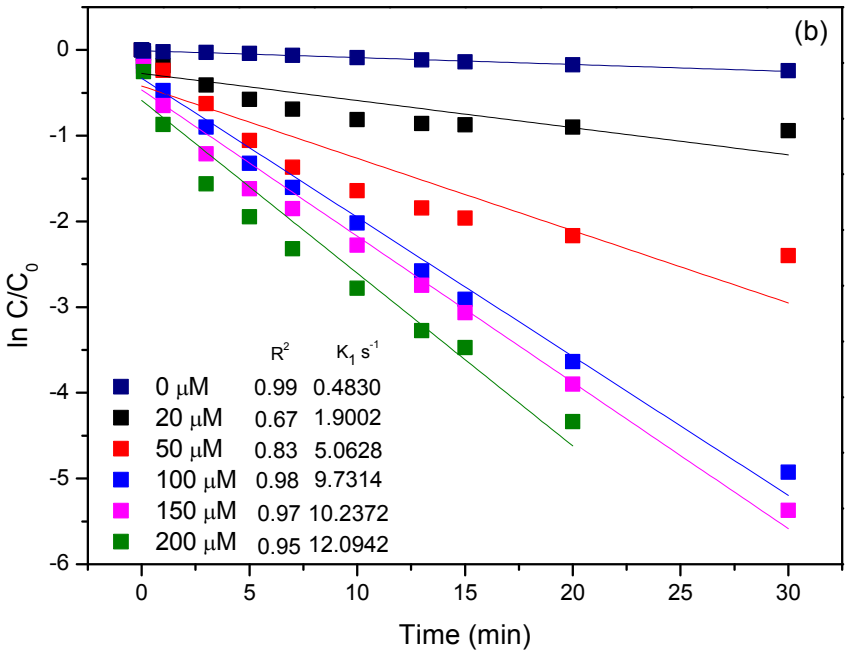

Figure S20. Effect of PM dosage on the degradation ratio (a) and reaction kinetics (b) of DCF by E-PM-Mn^{2+} process (Reaction conditions: initial DCF concentration=20 μM; initial pH=5; T=298±1 K; current=57 A m^{-2}; stirring speed=800 rpm; Mn^{2+} dosage=10μM).

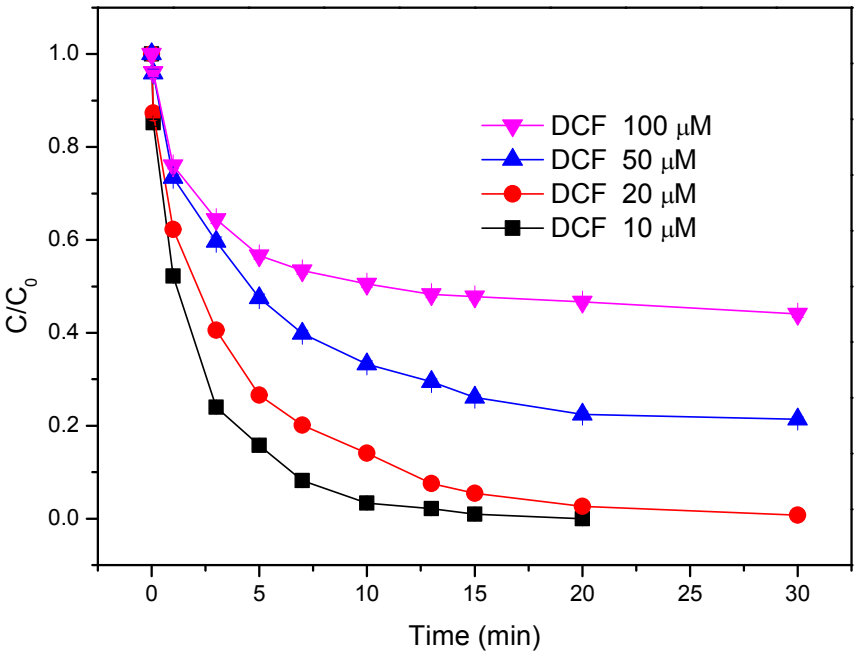

Figure S21. Effect of DCF concentration on the removal of DCF in E-PM-Mn^{2+} process (Reaction conditions: T=298±1 K; stirring speed=800 rpm; current=57 A m^{-2}; initial pH=5; PM dosage=100 μM; Mn^{2+} dosage=10 μM)

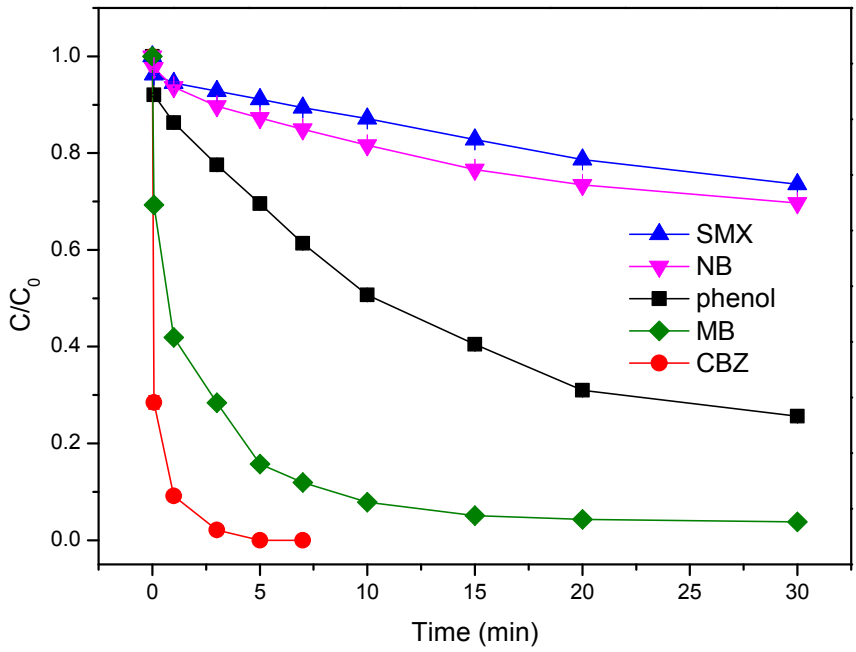

Figure S22. Removal of CBZ, phenol, SMX, NB, and MB in E-PM-Mn^{2+} process (Reaction conditions: initial contaminants concentration=20 μM; initial pH=5; T=298±1 K; current=57 A m^{-2}; stirring speed=800 rpm; PM dosage=100 μM; Mn^{2+} dosage=10 μM)

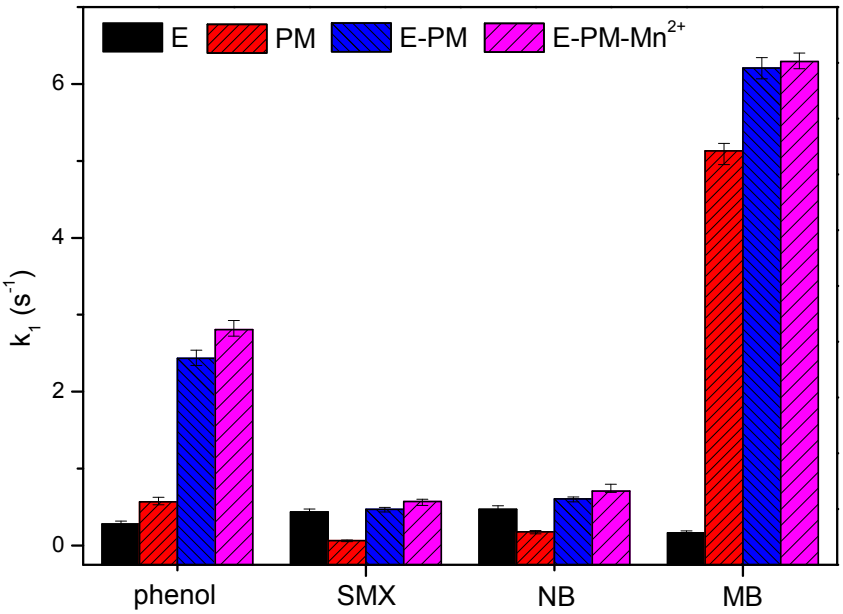

Figure S23. Degradation kinetics constants (k_1) of phenol, SMX, NB, MB in electrolysis (E), PM, E-PM, and E-PM-Mn^{2+} processes (Reaction conditions: initial contaminants concentration=20 μM; initial pH=5; T=298±1 K; current=57 A m^{-2}; stirring speed=800 rpm; PM dosage=100 μM; Mn^{2+} dosage=10 μM)

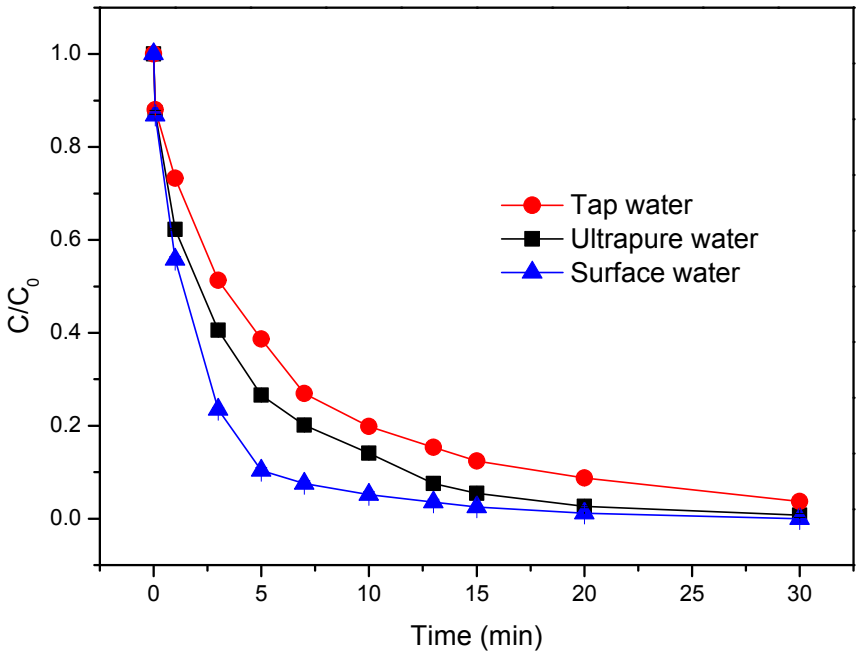

Figure S24. Effect of water matrices on the removal of DCF in E-PM-Mn^{2+} process (Reaction conditions: initial DCF concentration=20 μM; initial pH=5; T=298±1 K; current=57 A m^{-2}; stirring speed=800 rpm; PM dosage=100 μM; Mn^{2+} dosage=10 μM).

280

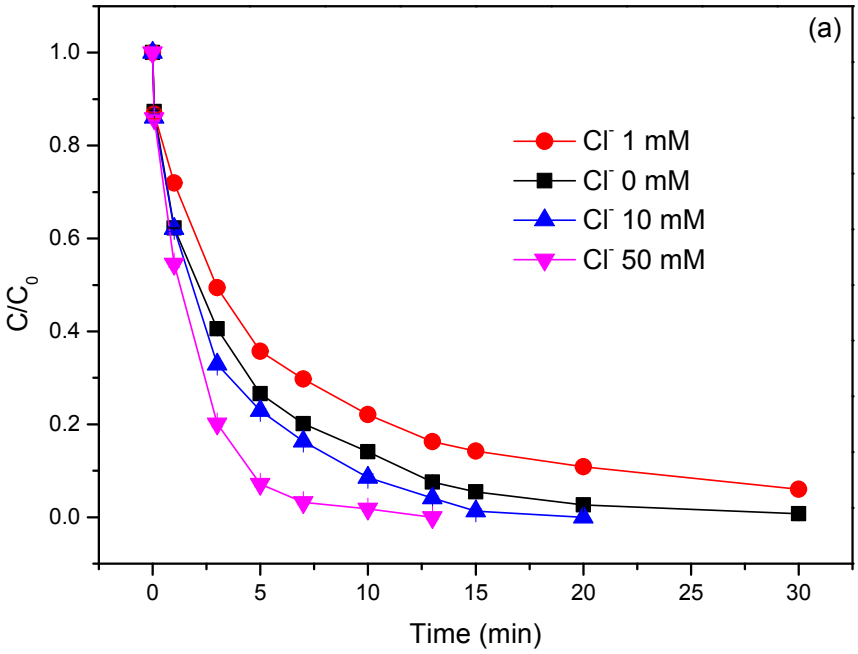
(a)
Cl- 1 mM
Cl- 0 mM
Cl- 10 mM
Cl- 50 mM
C/C0
Time (min)
0.0
0.2
0.4
0.6
0.8
1.0
0
5
10
15
20
25
30

281

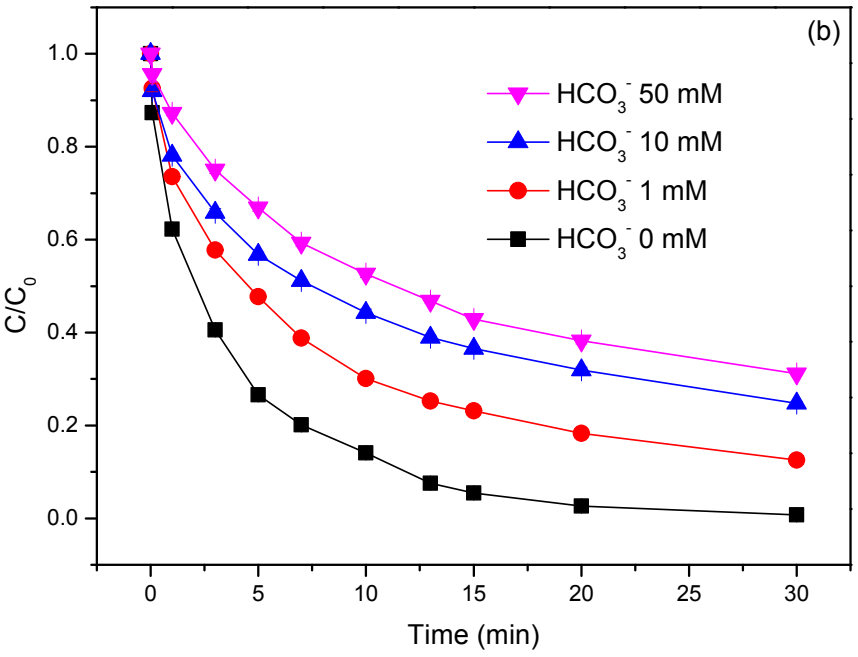
(b)
HCO3- 50 mM
HCO3- 10 mM
HCO3- 1 mM
HCO3- 0 mM
C/C0
Time (min)
0.0
0.2
0.4
0.6
0.8
1.0
0
5
10
15
20
25
30

282

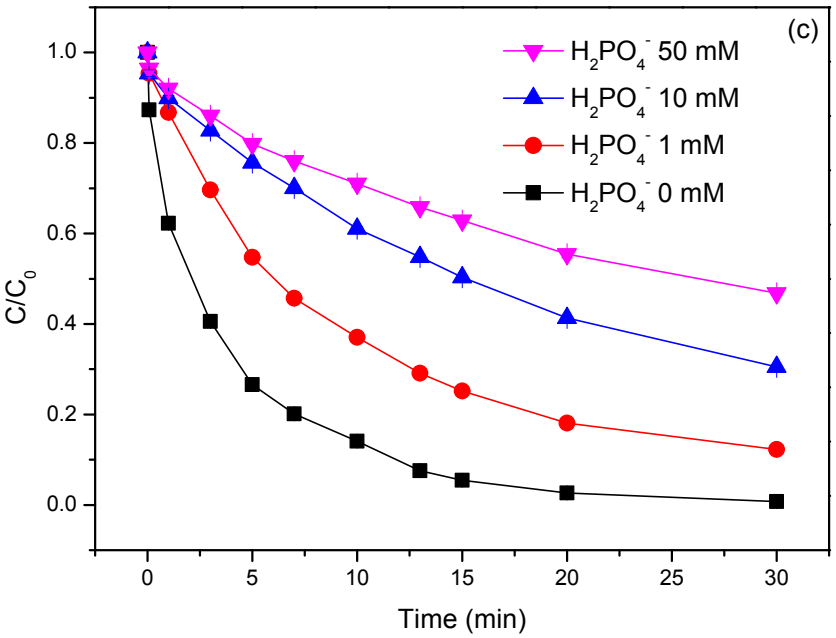

283

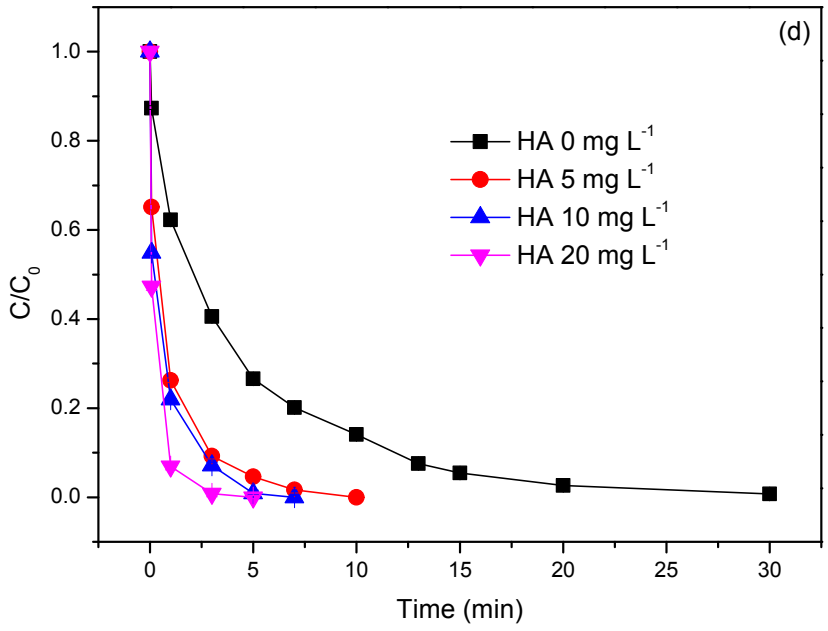

284

285 Figure S25. Effect of Cl^- (a), HCO_3^- (b), $H_2PO_4^-$ (c), and HA (d) on the degradation of

286 DCF in E-PM-Mn^{2+} process (Reaction conditions: initial DCF concentration=20 μM;

287 initial pH=5; T=298±1 K; current=57 A m^{-2}; stirring speed=800 rpm; PM dosage=100

288 μM; Mn^{2+} dosage=10 μM).

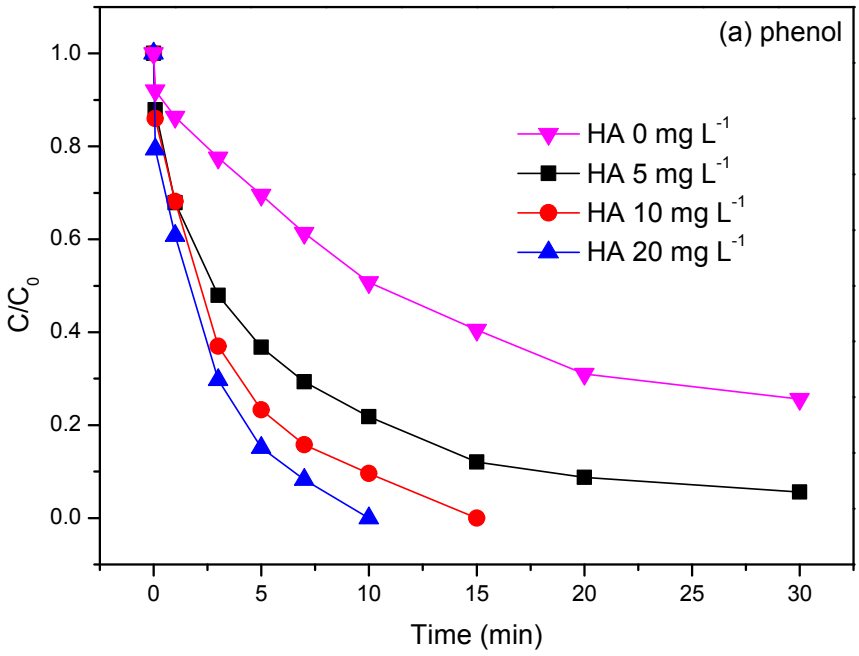
(a) phenol
HA 0 mg L-1
HA 5 mg L-1
HA 10 mg L-1
HA 20 mg L-1
C/C0
Time (min)
1.0
0.8
0.6
0.4
0.2
0.0
0
5
10
15
20
25
30

289

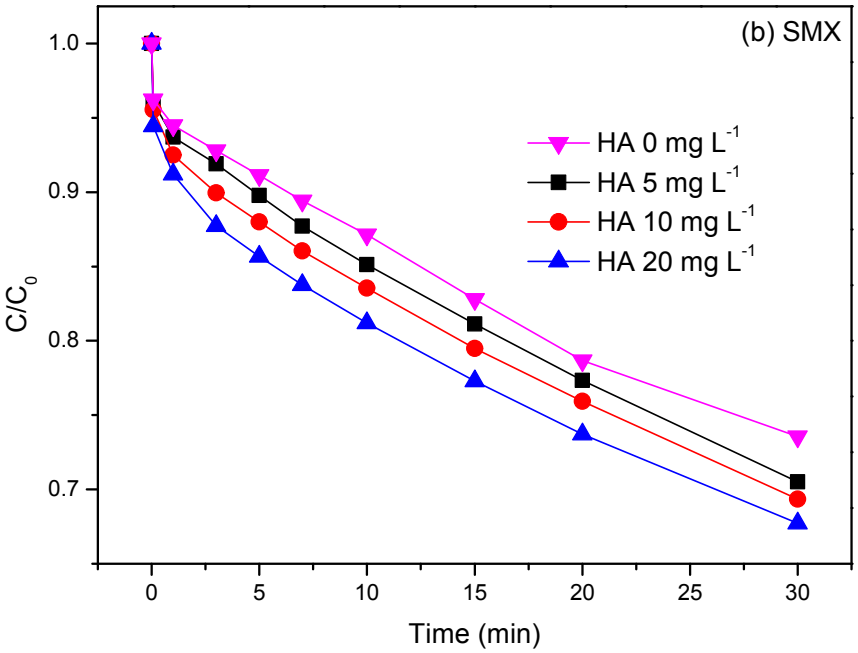
(b) SMX
HA 0 mg L-1
HA 5 mg L-1
HA 10 mg L-1
HA 20 mg L-1
C/C0
Time (min)
1.0
0.9
0.8
0.7
0
5
10
15
20
25
30

290

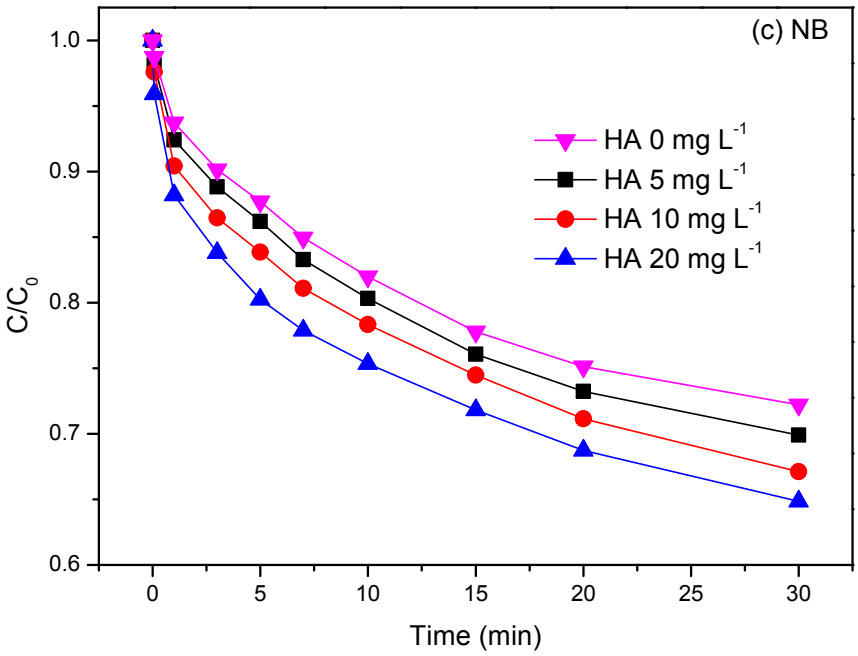

Figure S26. Effect of HA on the degradation of phenol (a), SMX (b) and NB (c) in E-PM-Mn^{2+} process (Reaction conditions: initial contaminant concentration=20 μM; initial pH=5; T=298±1 K; current=57 A m^{-2}; stirring speed=800 rpm; PM dosage=100 μM; Mn^{2+} dosage=10 μM; initial HA concentration=0, 5, 10, 20 mg L^{-1}).

REFERENCES

(1) Deng, J.; Shao, Y.; Gao, N.; Tan, C.; Zhou, S.; Hu, X. $CoFe_2O_4$ magnetic nanoparticles as a highly active heterogeneous catalyst of Oxone for the degradation of diclofenac in water. *J. Hazard. Mater.* **2013**, *262*, 836-844.

(2) Hua, Z.; Dai, Z.; Bai, X.; Ye, Z.; Wang, P.; Gu, H.; Huang, X. Copper nanoparticles sensitized TiO_2 nanotube arrays electrode with enhanced photoelectrocatalytic activity for diclofenac degradation. *Chem. Eng. J.* **2016**, *283*, 514-523.

(3) Khabbaz, M.; Entezari, M. H. Degradation of diclofenac by sonosynthesis of pyrite nanoparticles. *J. Environ. Manage.* **2017**, *187*, 416-423.

306 (4) Bagal, M. V.; Gogate, P. R. Degradation of diclofenac sodium using combined processes based on
307 hydrodynamic cavitation and heterogeneous photocatalysis. *Ultrason. Sonochem.* **2014**, *21*(3), 1035-
308 1043.
309 (5) Lu, X.; Shao, Y.; Gao, N.; Chen, J.; Zhang, Y.; Xiang, H.; Guo, Y. Degradation of diclofenac by
310 UV-activated persulfate process: kinetic studies, degradation pathways and toxicity assessments. *Ecotox.*
311 *Environ. Safe.* **2017**, *141*, 139-147.
312 (6) Dobrin, D.; Bradu, C.; Magureanu, M.; Mandache, N. B.; Parvulescu, V. I. Degradation of
313 diclofenac in water using a pulsed corona discharge. *Chem. Eng. J.* **2013**, *234*, 389-396.
314 (7) Bae, S.; Kim, D.; Lee, W. Degradation of diclofenac by pyrite catalyzed Fenton oxidation. *Appl.*
315 *Catal. B-Environ.* **2013**, *134*, 93-102.
316 (8) Nie, E.; Yang, M.; Wang, D.; Yang, X.; Luo, X.; Zheng, Z. Degradation of diclofenac by ultrasonic
317 irradiation: kinetic studies and degradation pathways. *Chemosphere* **2014**, *113*, 165-170.
318 (9) Garcia-Araya, J. F.; Beltran, F. J.; Aguinaco, A. Diclofenac removal from water by ozone and
319 photolytic TiO_2 catalysed processes. *J. Chem. Technol. Biot.* **2010**, *85*(6), 798-804.
320 (10) Beltran, F. J.; Pocostales, P.; Alvarez, P.; Oropesa, A. L. Diclofenac removal from water with
321 ozone and activated carbon. *J. Hazard. Mater.* **2009**, *163*(2-3), 768-776.
322 (11) Huang, T.; Zhang, G.; Chong, S.; Liu, Y.; Zhang, N.; Fang, S.; Zhu, J. Effects and mechanism of
323 diclofenac degradation in aqueous solution by US/Zn-0. *Ultrason. Sonochem.* **2017**, *37*, 676-685.
324 (12) Liu, S.; Zhao, X.; Zeng, H.; Wang, Y.; Qiao, M.; Guan, W. Enhancement of photoelectrocatalytic
325 degradation of diclofenac with persulfate activated by Cu cathode. *Chem. Eng. J.* **2017**, *320*, 168-177.
326